Quantifying biovariability in position and diameter of bridging veins to improve acute subdural hematoma prediction in FE head models

Rebeca Alejandra Gavrila Laic[a,d], Markos Kapeliotis[a,d], Nele Famaey[a], Bart Depreitere[b], Svein Kleiven[c], Jos Vander Sloten[a]

Abstract Bridging veins (BV) rupture is a major cause of Acute Subdural Hematoma. This study aims to quantify their biovariability to better understand their properties and increase the biofidelity of finite element (FE) head models. The number of BV and their measured diameters were manually counted in CT angiograms from 67 patients. A mixed linear model was used for the statistical analysis and the results were implemented in the KTH FE head model. LS-DYNA simulations were used to evaluate the amount of successful BV rupture predictions. The false positive and false negative predictions were also counted. The human brain has a mean of 23,18 BV, with diameters ranging between 0,37 and 3,24 mm. In the initial version of the KTH model two BV mechanical properties datasets gave a 6/8 successful prediction rate with one false positive and one false negative and one dataset gave a 7/8 successful prediction rate with one false negative. For the updated version all sets gave a 7/8 successful prediction rate with one false negative.
The number of BV and BV diameter size is segment dependent, but not hemisphere dependent. The implementation of these findings in the FE head model is a good preliminary attempt to increase BV rupture predictability.

Keywords acute subdural hematoma, bridging vein diameter, CT angiogram, finite element head model, head impact

I. INTRODUCTION

Bridging veins (BV) drain the blood from the cerebral cortex into the Superior Sagittal Sinus (SSS) (Vignes, Dagain, Guerin, & Liguoro, 2007) and they can be affected by mechanical forces applied to the brain. That will cause a relative movement of the brain inside the skull and could lead to their rupture (Depreitere et al., 2006), being a major cause of Acute Subdural Hematoma (ASDH) (Depreitere et al., 2006).
BV vulnerability towards ASDHs is strongly linked to the bridging vein mechanical properties (Gennarelli & Thibault, 1982; Vajtr et al., 2007), that depend on the structure and geometry of the vessel wall (Glagov, 1994). When BV rupture, blood flows creating a space under the dura mater and accumulates between the dura mater and the cortex (Depreitere et al., 2006), generating a blood clot that compresses the brain. This will last from hours to a few days (Nierenberger, Wolfram-Gabel, et al., 2013) and will lead very often to disastrous sequels, such as long term incapacity (Gennarelli & Thibault, 1982) and high mortality rates (Depreitere et al., 2006).
Despite the high importance of BV in the etiology of ASDH, not enough is known about their histological, morphological and mechanical properties (Famaey et al., 2015), mostly due to the high biovariability that characterizes these vessels. The knowledge of these properties is essential to better understand the vulnerability of BV (Nierenberger, Re, & Ahzi, 2013) and to create biofidelic finite element (FE) head models (Famaey et al., 2015; Kleiven, 2002). Finite elements models of the human head are one of the tools used to study head injuries such as ASDH. The wide majority of FE head models include a mechanical representation of bridging veins. The SIMon model (Takhounts et al., 2008) has BVs modelled as cable discrete beams with a Youngs modulus of 0.275 MPa. The KTH FE head model (Kleiven, 2007) has discrete beam elements with a stiffness of 1.9N, while the UCDBTM (Horgan & Gilchrist, 2003) and the WSUBIM (Viano et al., 2005) also have similar BV representations. There have been only a few studies investigating the reliability of head models on BV ruptures. One of the main parameters that can affect BV rupture is the diameter size. To the best of the authors knowledge, so far all models assign the same diameter size to every BV in the model.
CT angiography (CTA) is one of the most commonly used techniques for the evaluation of the brain vasculature, as it is fast (Pappu, Lerma, & Khraishi, 2016), it has high spatial resolution, and there is the possibility of creating various kinds of reconstructions in all desired planes (Dirnhofer, Jackowski, Vock, Potter, & Thali, 2006; Gao, Wang, Xiong, & Chen, 2016).

a Biomechanics Section, KU Leuven, Belgium. b Department of Neurosurgery, University Hospitals Leuven, Leuven, Belgium. c Division of Neuronic Engineering, Royal Institute of Technology (KTH), Huddinge, Sweden. d These authors contributed equally. Corresponding author: Rebeca Alejandra Gavrila Laic, e-mail: rebecaalejandra.gavrilalaic@kuleuven.be

Previous studies have shown that the anatomy of BV is quite variable (Famaey et al., 2015; Monea et al., 2014). The mean number of BV reported in literature is 12.3± 3.3 (males 12.9± 2.6, females 11.7± 3.8) per hemisphere, with a range of 7-20 BV (Brockmann, Kunze, Schmiedek, Groden, & Scharf, 2012). BV diameters range between 0.5-5.3 mm (K Oka, Rhoton, Barry, & Rodriguez, 1985), changing significantly depending on the location along the vein (Yamashima & Friede, 1984). However, anatomical and morphological characteristics of BV in the human brain, such as the distribution of BV along the SSS and the differences in diameters between different brain lobes, are still not clear (Chen et al., 2017a; Delye et al., 2006; Ehrlich, Maxeiner, & Lange, 2003; Lee & Haut, 1989; Li, Mahmood, Zhou, & Chopp, 2008; Monea et al., 2014; Monson, Goldsmith, Barbaro, & Manley, 2005; Kazunari Oka, Rhoton, Barry, & Rodriguez, 1985; Sampei, Yasui, Okudera, & Fukasawa, 1996; Vignes et al., 2007; Yamashima & Friede, 1984; Zhu, Wang, & Deng, 2018). Therefore, this study aims to provide the necessary anatomical description of BVs inter-subject diameter and distribution differences. This knowledge will be very useful to increase biofidelity in FE head models in the future.

II. METHODS

CTA from 67 patients (31 females, 36 males; age ranging from 24-89 years; mean age 60,75 years (SD 19,79), without previous history of neurovascular or neurological condition, taken in the context of routine clinical practice in University Hospitals Leuven (UZ Leuven), were collected, anonymized, and individually studied in the software MIMICS Research 19.0 (Materialise NV) by one researcher, who was blinded to the age and clinical status of the patient.

CTA were performed with an injected volume of contrast of 100 ml and a concentration of 350 mgI/ml. Whole stack images were used. Following the methodology of Musigazi *et al*, the cerebral cortex of each patient was divided in 10 equal segments, considering the inion and the nasion as reference points (Musigazi & Depreitere, 2015). The lines that separated the segments were placed at 18° one from the other. Segments 1-4 correspond to the frontal lobe, segments 5-8 to the parietal lobe and segments 9-10 to the occipital lobe (Musigazi & Depreitere, 2015).

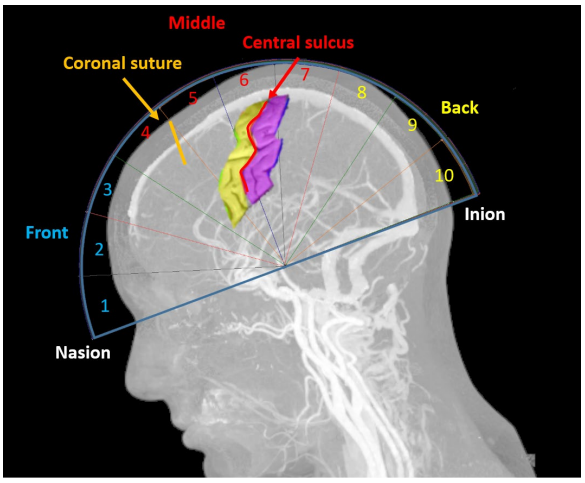

Figure 1: CT scan with the cerebral cortex divided in 10 segments

The number of BV found in each segment, together with their measured diameters at the SSS-BV connection point and at 1 cm proximal to the SSS, for both hemispheres, were manually counted by one researcher with biomedical training and supervised by a medical doctor. Diameters were measured with the `measure diameter' tool in MIMICS Research 19.0 (Materialise NV), using the predefined threshold sets for Soft Tissue CT provided by MIMICS Research 19.0 (Materialise NV). A graphical representation of the diameters' measurement can be observed in Supplementary Material [Figure 2].

All the results were registered in Excel. The total number of BV, mean diameter, SD, Median, Min and Max values were calculated for each segment individually and for the frontal, parietal and occipital lobes in Excel. Diameter measurements in the SSS were compared to the measurements taken at 1 cm proximal to the SSS.

Given that previous studies found no statistically significant differences in the number and size of BV between the right and left hemisphere (Han, Tao, & Zhang, 2007; Khuman et al., 2011), a test of fixed effects in SAS was used in our cohort to test if there were differences in the number of BV, distribution along the SSS and diameters between both hemispheres. The hemispheres were considered as independent variables in our statistical analysis. The probability for the presence of BV in the 10 different segments was calculated by dividing the number of observations of 1 or more BV per segment by the number of hemispheres studied. The probability for having only 1 BV and 2 or more BV per segment was also calculated by dividing the number of observations of 1 BV or 2 BV or more, respectively, per segment by the number of hemispheres studied. The probability of not having BV in the segment was calculated by dividing the number of times that no BV were observed, by the number of hemispheres studied. The percentages of diameter diminution at 1 cm proximal to the SSS were calculated dividing the diameters measured at 1 cm proximal to the SSS and the diameters registered in the SSS-BV connection point in the same vein [Fig 7].

A statistical analysis was performed with a SAS PROC MIXED model (Dickey, 2008), developed by the Leuven Statistics Research Center (LSTAT), in order to estimate the overall relations in the number and diameter size of BV between the 10 different segments. This model allowed us to fit a mixed effects model by maximum likelihood (Bates, n.d.), getting estimates of the variance components (Dickey, 2008). P values lower than 0.05 were considered to indicate a statistically significant difference.
The obtained results were implemented in the KTH FE head model (Kleiven, 2002). The Youngs modulus and diameter size reported by Delye (Delye et al., 2006), Monea (Monea et al., 2014) and Monson (Monson et al., 2005) were used to model the BV. The diameter sizes were adapted according to the CTA findings. More specifically, the percentage difference of the diameter size of the BV per lobe in the CTA dataset was calculated and then that percentage was applied to the three datasets in order to create models with lobe specific diameter sizes [Table 3]. Therefore, 3 non-lobes specific models (NLS) and 3 lobe specific models were developed using the aforementioned BV properties datasets. As rupture criterion the ultimate strain reported by each study was used [Table 1]. The strain calculated was the engineering strain and the peak strain was the maximum positive strain value of all BVs over the duration of the entire simulation. The experiments performed by Depreitere et al. 2006 were simulated in LS-DYNA using both the non-lobe specific models (NLS) and the lobe specific models (LS), upon which the amount of successful BV rupture predictions was evaluated. In the experiments 18 impacts were performed on 10 cadavers. When no rupture was produced from the initial impact the cadaver was impacted again. With respect to the second impacts, because the damage of the initial impact cannot be accounted for, the second impacts are not taken into consideration. Furthermore, 2 out of the 10 initial impacts were excluded because the data quality issues. All rupture sites are located in the pre and post Rolandic region. This area corresponds to the yellow and purple area in Figure 1 and should include segments 4, 5, 6 and 7. The objective was to evaluate how many successful predictions the lobe specific models can produce.

III. RESULTS

3.1. Number and diameter size of BV in the hemispheres

In our cohort, 832 BV were found in the right hemisphere and 749 BV in the left hemisphere. The boxplots show the number of BV found in each segment, for the left and right hemisphere, where RS is representing the right hemisphere segments and LS the left [Fig 3]. The BV mean diameters found in the SSS are shown for each segment and both hemispheres [Fig 4].
A comparison of the mean diameters found in each segment, in the right and left hemisphere, was performed with our SAS PROC MIXED model. The results showed no statistically significant differences between them (p 0.6271).

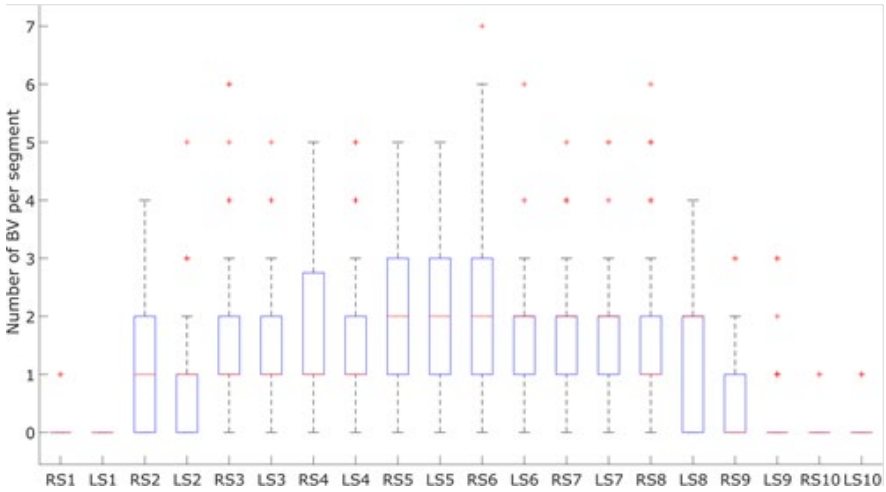

Figure 3: The number of observed BV per segment in the hemispheres. The highest number of BV is located in the parietal region, especially in segment 5, while the lowest number of BV is located in the occipital region

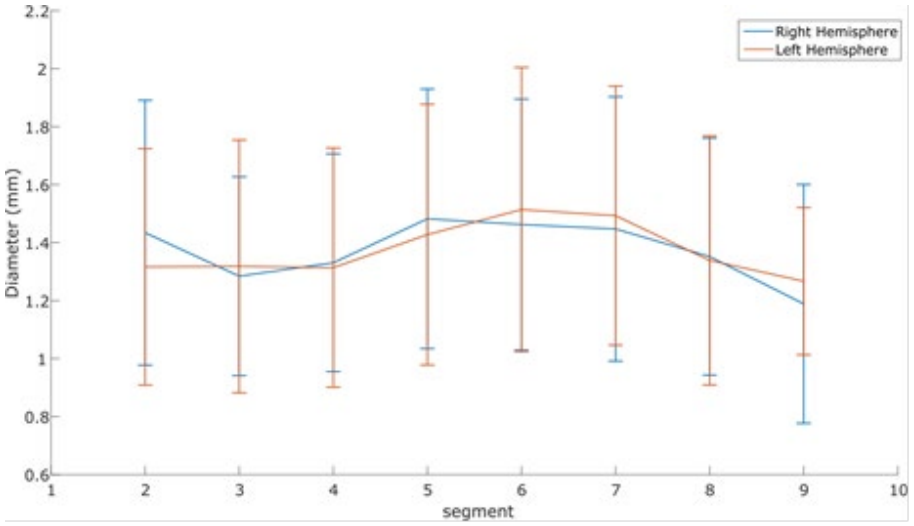

Figure 4. Mean diameter of the BV in the SSS per segment in hemispheres. They range between 1.22 mm and 1.72 mm, being the mean diameter for the cohort 1.40 mm.

3.2. Number of BV along the SSS

A total of 1581 BV, distributed along the 10 segments in which we divided the cerebral cortex, were studied in our cohort [Fig 5].

For the frontal, parietal and occipital lobe, the number of BV found in our cohort was 547, 977 and 57, respectively [Fig 6]. Within our cohort, there was a mean of 11,59 BV per brain hemisphere, ranging from 1 to 30 (SD 5,32), and a mean of 23,18 BV per brain, with a range from 2 to 48 (SD 9,49).

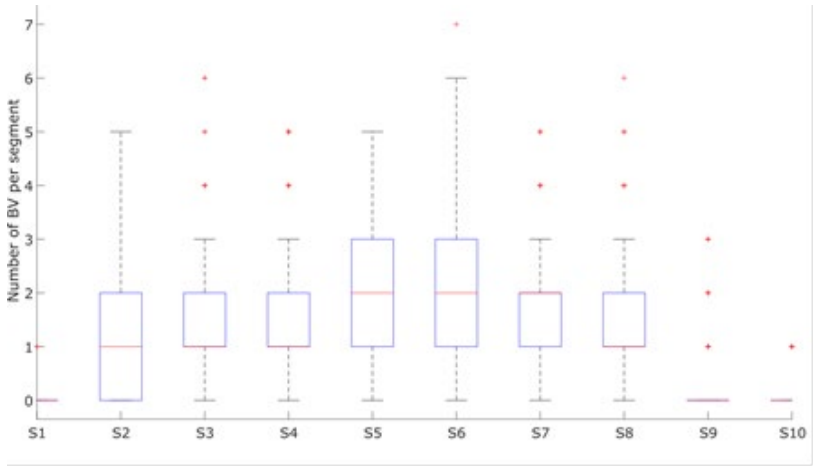

Figure 5: The number of BV per segment for both hemispheres combined. The highest number of BV can be seen in segments 5 and 6, while the lowest number of BV can be seen in segments 9 and 10.

3.3. Probability for the presence of BV in the different segments in the SSS

A total of 134 brain hemispheres were studied in our cohort. The probability for the presence of BV, for having only 1 BV and for having 2 or more BV in the 10 different segments was calculated. [Table 3 and Fig 7].

3.4. Mean diameter of BV along the SSS

The BV diameters, measured in each segment at the SSS-BV connection point ranged between 1,22-1,72 mm [Fig 4 and table 4].

The mean BV diameters per segment for the hemispheres can be seen in Figure 10.

The mean diameter at the SSS-BV connection point was 1.33 mm (SD 0.40; range 0.52-3.15 mm) in the frontal lobe, 1.44 mm (SD 0.45; range 0.37-3.09 mm) in the parietal lobe and 1.26 mm (SD 0.45; range 0.54-3.24 mm) in the occipital lobe. Considering the three lobes together, the mean diameter is 1.40 mm (SD 0.44; range 0.37-3.24 mm)[Fig 8].

After calculating the percentages of diameter diminution at 1cm proximal to the SSS we can see that there is a mean reduction in diameter of a 3% in the brain, which ranges from a diminution of 21% to a diminution of 2% in the different brain lobes, if we consider them separately [Fig 9].
The mean BV diameters per segment for the 134 hemispheres can be seen in Figure 10. The mean observed diameters in the 10 different segments, for our two reference locations can be seen in Supplementary Material [Figure 11].
The results obtained by the Differences of Least Squares Means test, included in our SAS PROC MIXED MODEL in order to know whether the differences in this comparison were statistically significant, are shown in Supplementary Material [Table 1].

TABLE I
BV MECHANICAL PARAMETERS REPORTED IN LITERATURE

	σu [MPa]	ε u [%]	E [MPa]
Delye	4.99±2.55	25.00± 8.00	30.69± 19.40
Monea	4.19±2.37	29.82± 13.26	25.72± 15.86
Monson	1.32±0.62	50.00± 19.00	6.43± 3.44

TABLE II
BV DIAMETER SIZE FOUND IN LITERATURE

	Mean Diameter [mm]	Frontal mean diameter [mm]	Parietal mean diameter [mm]	Occipital mean diameter [mm]
Delye	2.71	2.61	2.83	2.47
Monea	3.42	3.30	3.57	3.12
Monson	1.84	1.77	1.92	1.68

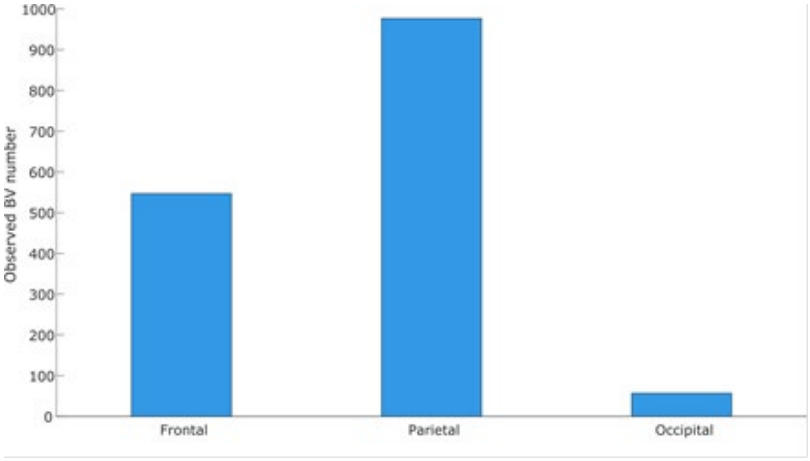

Figure 6: Total number of BV in the frontal, parietal and occipital lobe

The results show that at the SSS-BV connection point there are statistically significant different diameters within the frontal lobe, between the frontal and the parietal lobe, within the parietal lobe, between the frontal and the occipital lobe and between the parietal and the occipital lobe (Supplementary Material [Table 1]).
The predicted mean diameter was also obtained by the SAS PROC MIXED model [Supplementary Material [Fig 11]], which will be very useful in the future for finite element (FE) modelling of the BV. This predicted mean diameter ranges between 1,2 and 1,6 mm.

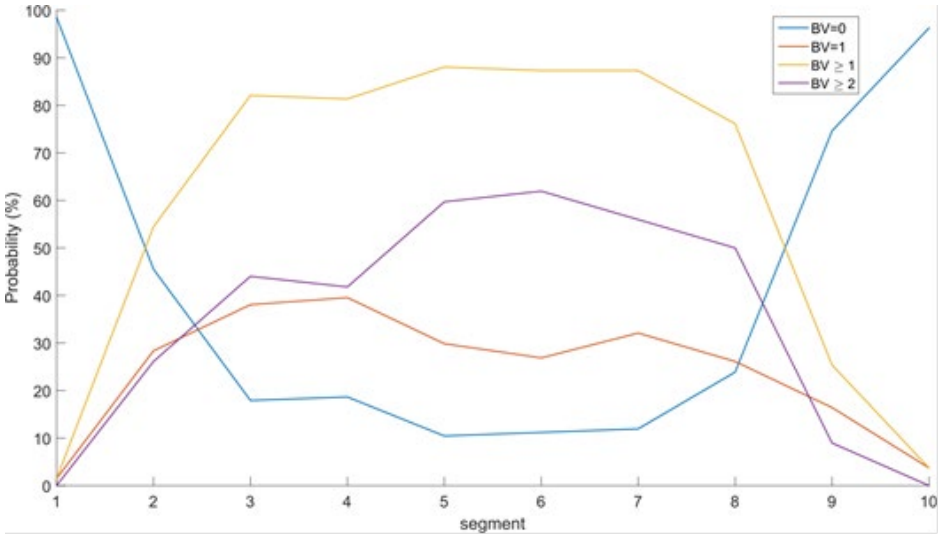

Figure 7: Probability for the presence of BV in the different segments. The parietal region has the highest probability for the presence of BV and the occipital region the lowest.

TABLE III
PROBABILITY FOR THE PRESENCE OF BV IN THE DIFFERENT SEGMENTS

	S 1	S 2	S 3	S 4	S 5	S 6	S 7	S 8	S 9	S 10
Observed BV_1	2	73	110	109	118	117	117	102	34	5
Probability (%) BV_1	1%	54%	82 %	81 %	88 %	87 %	87%	76%	25%	4%
Observed BV=1	2	38	51	53	40	36	43	35	22	5
Probability (%) BV=1	1%	28%	38%	40%	30%	27%	32%	26%	16%	4%
Observed BV_2	0	35	59	56	80	83	75	67	12	0
Probability (%) BV_2	0%	26%	44%	42%	60%	62%	56%	50%	9%	0%
Observed BV=0	132	61	24	25	14	15	16	32	100	129
Probability (%) BV=0	99%	46%	18%	19%	10%	11%	12%	24%	75%	96%

TABLE IV
MEAN DIAMETERS (MM) OF THE BV MEASURED IN THE SSS-BV CONNECTION POINT FOR THE DIFFERENT SEGMENTS

Segment	1	2	3	4	5	6	7	8	9	10
Mean diameter (mm) at the SSS-BV connection point	1,48	1,38	1,30	1,32	1,46	1,49	1,47	1,35	1,22	1,72

The differences between the different segments can be seen in Supplementary Material [Table 1].
Comparing the measurements taken at 1 cm proximal to the SSS-BV connection point, BV diameters are statistically significantly different between the frontal and the parietal lobe, within the parietal lobe, and between the parietal and occipital lobe (Supplementary Material [Table1]). The differences between the different segments can be observed in Supplementary Material [Table 1].
For the comparison of the BV diameter measurements at the SSS-BV connection point and 1 cm proximal to it, in the same segment, differences are only statistically significant in Segment 2 (Supplementary Material [Table 1]).

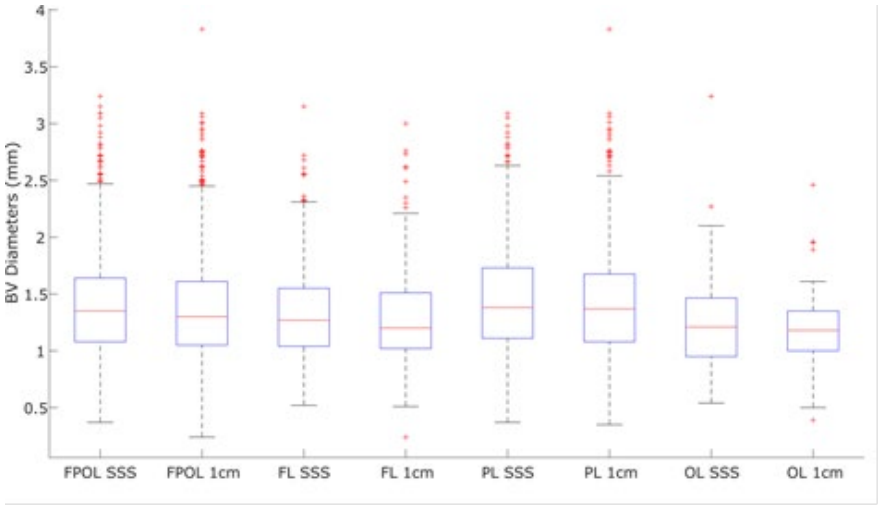

Figure 8: Box plots for the BV diameters, measured at the SSS-BV connection point and at 1cm proximal to the SSS, for the brain (FPOL), frontal lobe (FL), parietal lobe (PL) and occipital lobe (OL)

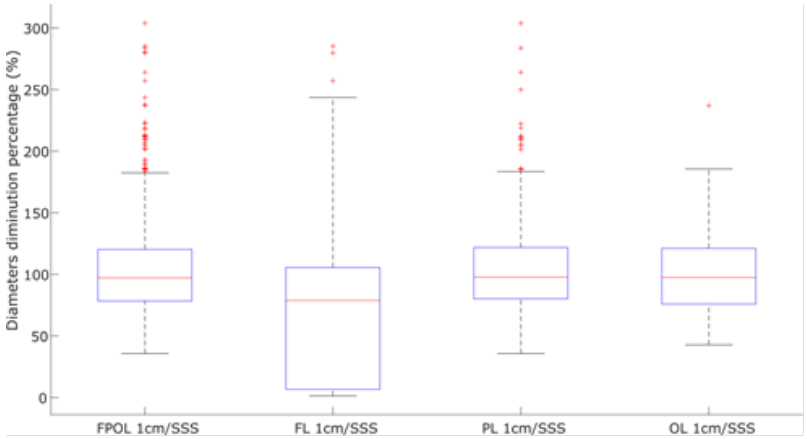

Figure 9: Box plots for the percentage of BV diameter decreasing at 1 cm proximal to the SSS, for the brain (FPOL),frontal lobe (FL), parietal lobe (PL) and occipital lobe (OL)

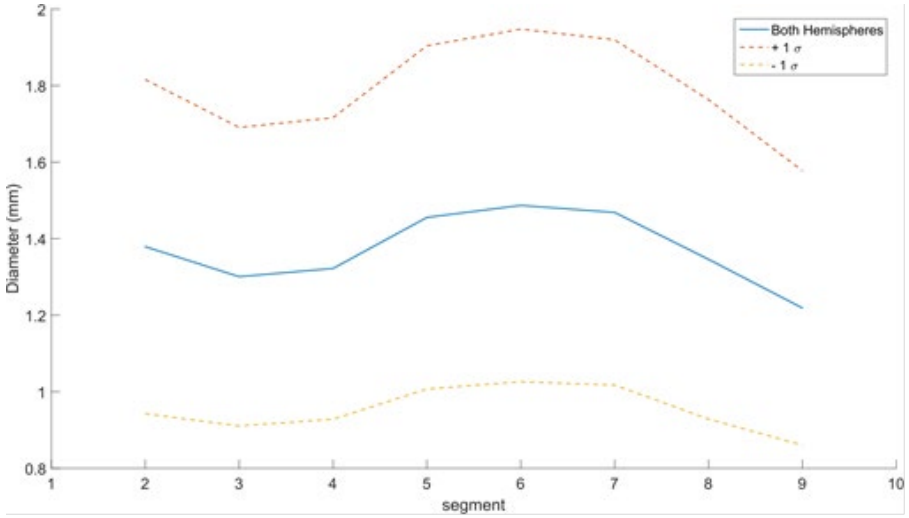

Figure 10: Mean diameter of the BV per segment for both hemispheres. We can see that BV located in the parietal region have bigger diameters than those located in the frontal and occipital regions.

3.5.Simulation results – Lobe specific model

The resulting comparison between the initial or Non-lobe specific model (NLS) and the lobe specific (LS) model is shown in table 5. The rupture criterion is the mean ultimate strain (μ), the mean ultimate strain minus one standard deviation (μ-σ) or the mean ultimate strain plus one standard deviation (μ+σ). The success rate is the percentage of the correct predictions over the total number of experiments.

TABLE V
Rupture prediction results between NLS and LS models

Model	BV properties	μ-σ	μ	μ+σ
NLS	Delye	75%	75%	75%
	Monea	75%	88%	88%
	Monson	75%	75%	75%
LS	Delye	75%	88%	88%
	Monea	75%	88%	88%
	Monson	75%	88%	88%

The results of each individual case are shown for all models in table 6.
For each set the false positive and false negative predictions were counted along with the successful predictions. In the initial version of the KTH model two sets gave a 6/8 successful prediction rate with one false positive and one false negative and one set gave a 7/8 successful prediction rate with one false negative. For the lobe specific version all sets gave a 7/8 successful prediction rate with one false negative.

IV. DISCUSSION

A total of 1581 BV were evaluated along the SSS in our cohort. Our results show that in the human brain there is a mean of 23.17 BV, with a range from 2 to 48 (SD 9.49), and a mean of 11.59 BV per brain hemisphere, ranging from 1 to 30 (SD 5.32).
These results are consistent with the results obtained by Han et al. (Han et al., 2007). However, we found bigger ranges than those shown in literature. Brockmann et al. (Brockmann et al., 2012) found a range from 7-20 BV per hemisphere, while Ehrlich et al. (Ehrlich et al., 2003) found a range from 9 to 31 BV per brain. Regarding the distribution of BV along the SSS, we found differences in the BV distribution in the different brain lobes. The parietal lobe, especially segment 5, is the region where we found the highest number of BV, while the occipital lobe was the region where we found the lowest number of BV. This uneven distribution of BV along the SSS has also been previously described in literature by Han et al (Han et al., 2007), who have stated that this is the reason why, with whatever movement of the brain in relation to the skull, there is a risk of rupture of BV leading to acute subdural hematoma.
Previous studies performed in cadavers have shown that veins in the rolandic or prerolandic areas tend to tear with rotational acceleration (Depreitere et al., 2006) and that the parietal region, where the highest number of BV are located, is also the most frequent region of BV rupture and ASDH (Depreitere et al., 2006; Kapeliotis et

TABLE VI
Simulation results obtained in each individual case for all models

Case	Model	Delye			Monea			Monson		
		RP	M. Str	Loc	RP	M. Str	Loc	RP	M. Str	Loc
01-3_1	NLS	FP	27.2%	M	SP	26.0%	M	FP	73.2%	B
	LS	SP	24.9%	M	SP	24.6%	M	SP	41.5%	F
21-3_1	NLS	SP	5.3%	B	SP	3.1%	B	SP	11.7%	B
	LS	SP	3.8%	B	SP	3.6%	B	SP	8.0%	B
22-3_1	NLS	SP	5.9%	B	SP	4.4%	B	SP	10.2%	B
	LS	SP	5.2%	B	SP	4.8%	B	SP	8.7%	B
25-2_1	NLS	SP	6.7%	B	SP	6.2%	B	SP	10.8%	F
	LS	SP	6.0%	B	SP	5.8%	B	SP	9.5%	F
28-2_1	NLS	FN	10.2%	B	FN	9.9%	B	FN	18.8%	B
	LS	FN	10.0%	B	FN	9.6%	B	FN	17.6%	B
29-3_1	NLS	SP	47.5%	B	SP	87.9%	B	SP	139.5%	B
	LS	SP	46.1%	B	SP	81.9%	B	SP	130.4%	B
30-2_1	NLS	SP	7.8%	B	SP	7.7%	B	SP	16.4%	B
	LS	SP	6.7%	B	SP	6.4%	B	SP	12.6%	B
32-2_1	NLS	SP	8.5%	B	SP	6.9%	B	SP	17.1%	B
	LS	SP	7.4%	B	SP	7.1%	B	SP	13.3%	B

RP = rupture prediction, M. Str = maximum strain, Loc = maximum strain location
SP = successful prediction, FP = false positive, FN = false negative

al., 2019).

Given that BV are unevenly distributed along the SSS, we decided to calculate the probability for the presence of BV in the different brain regions, which is an operation that has not been previously shown in literature and would be very important for BV representation in FE head models. Changing the position of BV in the FE model and implementing different diameters in the different lobes is a straightforward adaptation of the model that will affect the observed BV stresses and strains.

Our results show that there is a higher probability to have BV in the parietal lobe, than in the occipital and frontal lobes, in the SSS. Moreover, in the SSS there is a higher probability of having only 1 BV per segment in the frontal and occipital lobe, while in the parietal lobe there are higher chances of having ≥2 BV per segment.

The study of the distribution of BV was complemented with the manual measurement of the diameter in all the BV found in the CTA scans of the patients in our cohort. A major limitation is that in CTA images the only visible part is the lumen of the vein. This is the reason why instead of using the actual measurements of the BV in the KTH head model we use the percentage difference of BV diameter obtained in our study. In this way, we use the measured diameters and mechanical properties from each individual study but we also add the lobe specificity that was observed in our findings. Furthermore, we did not have the possibility to consider the thickness of the BV wall in our BV diameters measurement. The wall thickness of the BV that is considered in the original KTH model was also adjusted according to the same percentage difference. To the best of the authors knowledge, there is no imaging technique with a high enough resolution to capture the wall thickness of BV in in vivo patients. Furthermore, this evaluation has been manually done by one researcher and, therefore, user-dependent. However, despite these limitations, these results provide very useful information about anatomical and morphological properties of BV.

BV diameters in our cohort ranged between 0.37 and 3.24 mm, while slightly larger diameters, ranging between 0.5 and 5.8 mm, were reported in other studies (Chen et al., 2017b; Delye et al., 2006; Ehrlich et al., 2003; Lee & Haut, 1989; Monea et al., 2014; Monson et al., 2005; Sampei et al., 1996; Vignes et al., 2007; Yamashima & Friede, 1984; Zhu et al., 2018) [Table 4, Fig 7]. The pixel size of the available CTA ranged from 0.24 to 0.86 mm with a mean of 0.5 mm.

Previous studies have described that BV diameters change significantly depending on their location in the vein (Famaey et al., 2015). Thus, we decided to consider one more measurement point, 1 cm proximal to the SSS, in order to see how diameter changes within the same vein. Our results show a mean diameter of 1.28 mm (SD 0.38) in the frontal lobe, of 1.42 mm (SD 0.47) in the parietal lobe and of 1.20 mm (SD 0.37) in the occipital lobe. A minor diameter difference of 3% has been observed between the SSS and 1 cm proximal to the SSS when considering all the lobes together, while a 21% diameter diminution was found when calculating the differences in the FL.

That was also observed in our SAS PROC MIXED model. There, we saw that only the changes in diameter throughout the length of the vessel were statistically significant in segment 2. Even though we see a tendency for a decrease of 3% in the diameter towards the brain end of the vein in the SSS, we only found statistically significant differences for one of the ten segments.

Our results have demonstrated that the number and diameters of BV in the SSS, do not have statistically significant differences between the left and right hemisphere. However, they have statistically significant differences between the frontal, parietal and occipital lobe, with the parietal lobe being the one with the highest number and the bigger diameters of BV, and the occipital lobe the one with the lowest number and smallest diameters.

These results will be very useful in the future to increase the biofidelity of BV in FE head models and to allow reliable prediction of ASDH due to BV rupture that is necessary, given its high prevalence (Attwell & Laughlin, 2001) and needs to be achieved by a more extensive study of anatomical, morphological and mechanical properties in these veins (Famaey et al., 2015). FE simulation has been used in the past years to investigate injury mechanics and can predict head responses and injuries in different impact situations (Famaey et al., 2015).

Furthermore, the lobe specific models showed that there was an improvement in the predictive capability of BV rupture. Out of the 8 cases in total, there was only one false negative and one false positive result when the initial NLS model was used. From these two false results, the false positive case prediction was eliminated from all datasets in the newly adapted LS model. In that same case for the set of Monson *et al* 2005 , the lobe specific maximum strain prediction was at segment 3 which is closer to the prerolandic area than segment 9 in the non-lobe specific model. This is another indication that increasing biofidelity in BV representation can improve the predictive capability of FE head models, even though the rest of the maximum strain locations did not change

and remained at the occipital lobe for both models for the other cases. Which is contrary to results of the cadaver experiments that showed all ruptures located at the rolandic and prerolandic area that corresponds to the parietal lobe closer to the border with the frontal lobe. While more experiments like the experiments from Depreitere (Depreitere et al., 2006) would help modelers improve FE head models in ASDH prediction, for the moment and by using the available information we have at hand, this new adaptation is considered to be of value.

The KTH model adaptation of Zhou *et al* (Zhou, Li, & Kleiven, 2019), where the authors used an FSI approach to model cerebrospinal fluid, could have been an even more suitable approach to apply our findings with respect to BV anatomy. However, that model was considered at the time to be a rather heavy model to run and considering our resources we opted for the standard KTH model to use as a proof of concept. This is however a step that should be investigated in the future.

Different FE head models have been developed in the last decades (Kleiven, 2002; Roth, Raul, & Willinger, 2010). However, some of them do not include a mechanical representation of BV or do not include important anatomical considerations that would increase their biofidelity (Famaey et al., 2015). Some examples are the models developed in the Université de Strasbourg (UDS) (Roth et al., 2010) or the KTH FE head model (Kleiven, 2002). In the case of the models developed by UDS (Roth et al., 2010), they do not contain a mechanical representation of BV, while the KTH FE head model (Kleiven, 2002), includes 11 pairs of BV, that were modelled according to the anatomical descriptions of Oka et al. (Kazunari Oka et al., 1985). Applying in FE head models the findings concerning the distribution and diameter size of BV in different brain lobes will increase their biofidelity and improve their predictive capability w.r.t. ASDH.

However, those models do not consider the differences in BV distribution and diameters in the different brain lobes that will increase FE head models' biofidelity and which will be possible in the future considering our results.

Furthermore, these results can also be very important in neurosurgery, as bridging veins are used as landmarks in specific locations during neurosurgery (Mortazavi et al., 2013), and an improvement in the anatomical and morphological knowledge of BV could improve the quality of the procedures in this field.

V. CONCLUSIONS

The human brain has a mean of 23.18 BV (11.59 per hemisphere) distributed along the SSS, with diameters ranging between 0.37 and 3.24 mm, that differ in number and diameter between the frontal, parietal and occipital lobe in the SSS among patients. In the SSS, the parietal lobe has the highest number of BV, with the biggest diameters, while the occipital lobe has the lowest number of BV, with the smallest diameters. Therefore, the number of BV and BV diameter size is segment dependent, but not hemisphere dependent. There are no statistically significant differences in the number and diameters of BV in the SSS between the left and right hemisphere. Modelling these findings in the KTH head model was a good preliminary attempt to show an improvement in its predictive capability, making it clear that more biofidelity is needed in order to improve the overall predictive capability of the models.

VI. ACKNOWLEDGEMENT

The authors would like to thank Prof. Anne-Marie De Meyer and Leuven Statistics research center (LSTAT) for providing the PROC MIXED model which was used for the statistical analysis, and Dr. Gracia Umuhire Musigazi for providing useful insights in bridging vein anatomy and establishing the method used to categorize bridging veins with respect to their position.

VII. REFERENCES

Attwell, D., & Laughlin, S. B. (2001). An energy budget for signaling in the grey matter of the brain. *Journal of Cerebral Blood Flow and Metabolism : Official Journal of the International Society of Cerebral Blood Flow and Metabolism*, *21*(10), 1133–1145. https://doi.org/10.1097/00004647-200110000-00001

Bates, D. (n.d.). *lmer for SAS PROC MIXED Users*.

Brockmann, C., Kunze, S. C., Schmiedek, P., Groden, C., & Scharf, J. (2012). Variations of the superior sagittal sinus and bridging veins in human dissections and computed tomography venography. *Journal of Clinical Imaging*, *36*(2), 85–89. https://doi.org/10.1016/j.clinimag.2011.05.003

Chen, Y., Zhang, R., Lian, J., Luo, F., Han, H., & Deng, X. (2017a). Flow Dynamics of Cerebral Bridging Veins Entering Superior Sagittal Sinus by Color-Coded Duplex Sonography. *Journal of Medical Imaging and Health*

Informatics, *7*(4), 862–866. https://doi.org/10.1166/jmihi.2017.2095

Chen, Y., Zhang, R., Lian, J., Luo, F., Han, H., & Deng, X. (2017b). Flow Dynamics of Cerebral Bridging Veins Entering Superior Sagittal Sinus by Color-Coded Duplex Sonography. *Journal of Medical Imaging and Health Informatics*, *7*(4), 862–866.

Delye, H., Goffin, J., Verschueren, P., Vander Sloten, J., Van der Perre, G., Alaerts, H., … Berckmans, D. (2006). Biomechanical properties of the superior sagittal sinus-bridging vein complex. *Stapp Car Crash Journal*, *50*, 625–636.

Depreitere, B., Van Lierde, C., Sloten, J. Vander, Van Audekercke, R., Van der Perre, G., Plets, C., & Goffin, J. (2006). Mechanics of acute subdural hematomas resulting from bridging vein rupture. *Journal of Neurosurgery*, *104*(6), 950–956. https://doi.org/10.3171/jns.2006.104.6.950

Dickey. (2008). *PROC MIXED: Underlying Ideas with Examples*.

Dirnhofer, R., Jackowski, C., Vock, P., Potter, K., & Thali, M. J. (2006). VIRTOPSY: minimally invasive, imaging-guided virtual autopsy. *Radiographics : A Review Publication of the Radiological Society of North America, Inc*, *26*(5), 1305–1333. https://doi.org/10.1148/rg.265065001

Ehrlich, E., Maxeiner, H., & Lange, J. (2003). Postmortem radiological investigation of bridging vein ruptures. *Legal Medicine (Tokyo, Japan)*, *5 Suppl 1*, S225-7.

Famaey, N., Ying Cui, Z., Umuhire Musigazi, G., Ivens, J., Depreitere, B., Verbeken, E., & Vander Sloten, J. (2015). Structural and mechanical characterisation of bridging veins: A review. *Journal of the Mechanical Behavior of Biomedical Materials*, *41*, 222–240. https://doi.org/10.1016/j.jmbbm.2014.06.009

Gao, X., Wang, X., Xiong, W., & Chen, J. (2016). In vivo reprogramming reactive glia into iPSCs to produce new neurons in the cortex following traumatic brain injury. *Nature Publishing Group*, (March), 1–13. https://doi.org/10.1038/srep22490

Gennarelli, T. A., & Thibault, L. E. (1982). Biomechanics of acute subdural hematoma. *The Journal of Trauma*, *22*(8), 680–686.

Glagov, S. (1994). Intimal hyperplasia, vascular modeling, and the restenosis problem. *Circulation*, *89*(6), 2888–2891. https://doi.org/10.1161/01.CIR.89.6.2888

Han, H., Tao, W., & Zhang, M. (2007). The dural entrance of cerebral bridging veins into the superior sagittal sinus: an anatomical comparison between cadavers and digital subtraction angiography. *Neuroradiology*, *49*(2), 169–175. https://doi.org/10.1007/s00234-006-0175-z

Horgan, T. J., & Gilchrist, M. D. (2003). The creation of three-dimensional finite element models for simulating head impact biomechanics. *International Journal of Crashworthiness*, *8*(4), 353–366. https://doi.org/10.1533/ijcr.2003.0243

Kapeliotis, M., Musigazi, G. U., Famaey, N., Depreitere, B., Kleiven, S., & Sloten, J. Vander. (2019). The sensitivity to inter-subject variability of the bridging vein entry angles for prediction of acute subdural hematoma. *Journal of Biomechanics*. https://doi.org/https://doi.org/10.1016/j.jbiomech.2019.05.016

Khuman, J., Meehan, W. P. 3rd, Zhu, X., Qiu, J., Hoffmann, U., Zhang, J., … Whalen, M. J. (2011). Tumor necrosis factor alpha and Fas receptor contribute to cognitive deficits independent of cell death after concussive traumatic brain injury in mice. *Journal of Cerebral Blood Flow and Metabolism : Official Journal of the International Society of Cerebral Blood Flow and Metabolism*, *31*(2), 778–789. https://doi.org/10.1038/jcbfm.2010.172

Kleiven, S. (2002). *Finite element modeling of the human head*. Royal University of Technology.

Kleiven, S. (2007). Predictors for traumatic brain injuries evaluated through accident reconstructions. *Stapp Car Crash Journal*, *51*, 81–114.

Lee, M. C., & Haut, R. C. (1989). Insensitivity of tensile failure properties of human bridging veins to strain rate: implications in biomechanics of subdural hematoma. *Journal of Biomechanics*, *22*(6–7), 537–542.

Li, B. O., Mahmood, A., Zhou, D., & Chopp, M. (2008). of Neurogenesis Are Associated with Therapeutic Improvement after Traumatic Brain Injury INTRODUCTION, *139*(February), 130–139. https://doi.org/10.1089/neu.2007.0369

Monea, A. G., Baeck, K., Verbeken, E., Verpoest, I., Sloten, J. Vander, Goffin, J., & Depreitere, B. (2014). The biomechanical behaviour of the bridging vein-superior sagittal sinus complex with implications for the mechanopathology of acute subdural haematoma. *Journal of the Mechanical Behavior of Biomedical Materials*, *32*, 155–165. https://doi.org/10.1016/j.jmbbm.2013.12.007

Monson, K. L., Goldsmith, W., Barbaro, N. M., & Manley, G. T. (2005). Significance of source and size in the mechanical response of human cerebral blood vessels. *Journal of Biomechanics*, *38*(4), 737–744. https://doi.org/10.1016/j.jbiomech.2004.05.004

Mortazavi, M. M., Denning, M., Yalcin, B., Shoja, M. M., Loukas, M., & Tubbs, R. S. (2013). The intracranial bridging veins: a comprehensive review of their history, anatomy, histology, pathology, and neurosurgical implications. *Child's Nervous System : ChNS : Official Journal of the International Society for Pediatric Neurosurgery*, *29*(7), 1073–1078. https://doi.org/10.1007/s00381-013-2054-3

Musigazi, G. U., & Depreitere, B. (2015). Study of bridging vein anatomy based on CT angiogram data for optmization of finite element models simulating acute subdural hematoma. In *European Association of Neurosurgical Societies Annual Conference*. Madrid. Retrieved from https://academy.eans.org/eans/2015/madrid/109189/gracia.umuhire.musigazi.study.of.bridging.vein.anatomy.based.on.ct.angiogram.html

Nierenberger, M., Re, Y., & Ahzi, S. (2013). A new multiscale model for the mechanical behavior of vein walls. *Journal of the Mechanical Behavior of Biomedical Materials*, *23*, 32–43. https://doi.org/10.1016/j.jmbbm.2013.04.001

Nierenberger, M., Wolfram-Gabel, R., Decock-Catrin, S., Boehm, N., Remond, Y., Kahn, J.-L., & Ahzi, S. (2013). Investigation of the human bridging veins structure using optical microscopy. *Surgical and Radiologic Anatomy : SRA*, *35*(4), 331–337. https://doi.org/10.1007/s00276-012-1035-7

Oka, K, Rhoton, A. L. J., Barry, M., & Rodriguez, R. (1985). Microsurgical anatomy of the superficial veins of the cerebrum. *Neurosurgery*, *17*(5), 711–748.

Oka, Kazunari, Rhoton, A. L., Barry, M., & Rodriguez, R. (1985). Microsurgical Anatomy of the Superficial Veins of the Cerebrum. *Forensic Science International*, *17*(5).

Pappu, S., Lerma, J., & Khraishi, T. (2016). Brain CT to Assess Intracranial Pressure in Patients with Traumatic Brain Injury. *Journal of Neuroimaging : Official Journal of the American Society of Neuroimaging*, *26*(1), 37–40. https://doi.org/10.1111/jon.12289

Roth, S., Raul, J.-S., & Willinger, R. (2010). Finite element modelling of paediatric head impact: global validation against experimental data. *Computer Methods and Programs in Biomedicine*, *99*(1), 25–33. https://doi.org/10.1016/j.cmpb.2009.10.004

Sampei, T., Yasui, N., Okudera, T., & Fukasawa, H. (1996). Anatomic study of anterior frontal cortical bridging veins with special reference to the frontopolar vein. *Neurosurgery*, *38*(5), 971–975.

Takhounts, E. G., Ridella, S. A., Hasija, V., Tannous, R. E., Campbell, J. Q., Malone, D., … Duma, S. (2008). Investigation of traumatic brain injuries using the next generation of simulated injury monitor (SIMon) finite element head model. *Stapp Car Crash Journal*, *52*, 1–31.

Vajtr, D., Prusa, R., Kukacka, J., Houst'ava, L., Samal, F., Pelichovska, M., … Toupalik, P. (2007). [Evaluation of relevance in concussion and damage of health by monitoring of neuron specific enolase and S-100b protein]. *Soudni lekarstvi*, *52*(3), 43–46.

Viano, D. C., Casson, I. R., Pellman, E. J., Zhang, L., King, A. I., & Yang, K. H. (2005). Concussion in professional football: brain responses by finite element analysis: part 9. *Neurosurgery*, *57*(5), 891–916. https://doi.org/10.1227/01.neu.0000186950.54075.3b

Vignes, J.-R., Dagain, A., Guerin, J., & Liguoro, D. (2007). A hypothesis of cerebral venous system regulation based on a study of the junction between the cortical bridging veins and the superior sagittal sinus. Laboratory investigation. *Journal of Neurosurgery*, *107*(6), 1205–1210. https://doi.org/10.3171/JNS-07/12/1205

Yamashima, T., & Friede, R. L. (1984). Why do bridging veins rupture into the virtual subdural space? *Journal of Neurology, Neurosurgery, and Psychiatry*, *47*(2), 121–127.

Zhou, Z., Li, X., & Kleiven, S. (2019). Fluid-structure interaction simulation of the brain-skull interface for acute subdural haematoma prediction. *Biomechanics and Modeling in Mechanobiology*, *18*(1), 155–173. https://doi.org/10.1007/s10237-018-1074-z

Zhu, Y., Wang, F., & Deng, X. (2018). Hemodynamics of cerebral bridging veins connecting the superior sagittal sinus based on numerical simulation. *Biomedical Engineering Online*, *17*(1), 35. https://doi.org/10.1186/s12938-018-0466-8

SUPLEMENTARY MATERIAL

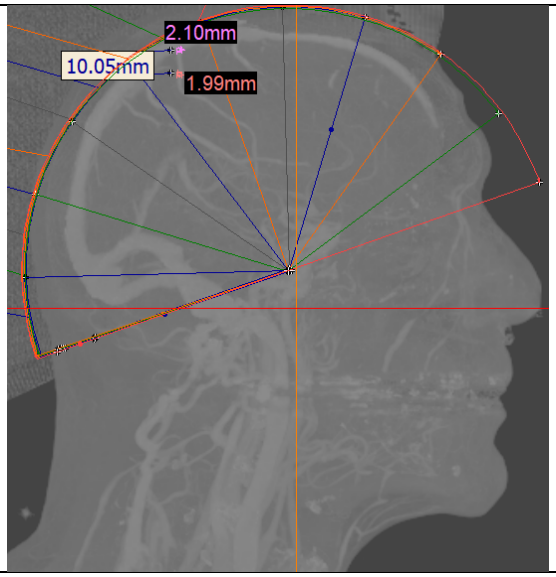

Figure 2: CT scan with a measured diameter at the SSS-BV connection point and at 1cm proximal to the SSS

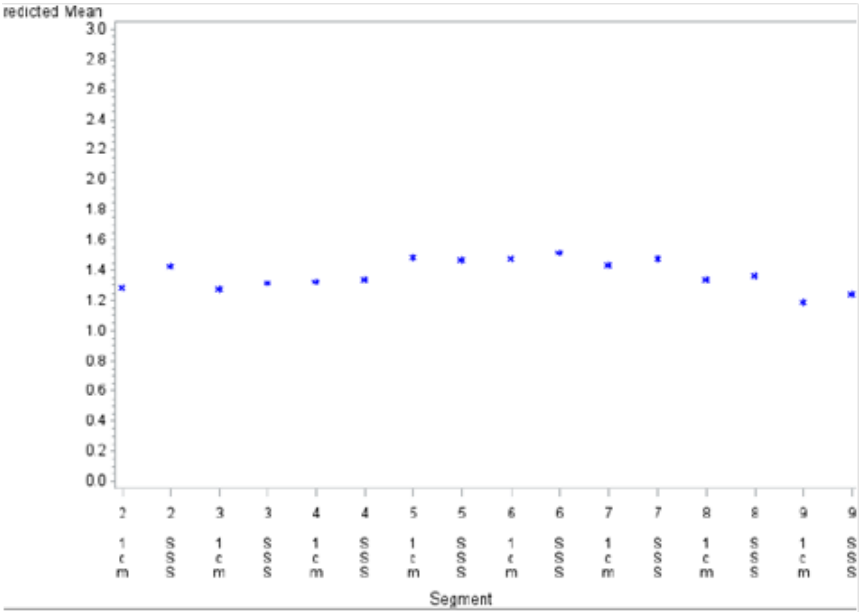

Figure 11: Predicted BV mean diameters at the SSS-BV connection point and at 1 cm proximal to the SSS in the 10 segments

Differences of Least Square Means

Table 1: Differences of Least Squares Means for the BV diameters at the SSS-BV connection point and 1 cm proximal to the SSS in the 10 different segments

S	S	Est.	SE	t Value	Pr > |t|
S 1 1cm	S 2 1cm	0.2346	0.2924	0.80	0.4225
S1 1cm	S 2 SSS	0.09488	0.2924	0.32	0.7456
S 1 1cm	S 3 1cm	0.2500	0.2913	0.86	0.3910
S 1 1cm	S 3 SSS	0.2037	0.2914	0.70	0.4846
S 1 1cm	S 4 1cm	0.1945	0.2914	0.67	0.5046
S 1 1cm	S 4 SSS	0.1847	0.2914	0.63	0.5262
S 1 1cm	S 5 1cm	0.04052	0.2911	0.14	0.8893
S 1 1cm	S 5 SSS	0.05288	0.2911	0.18	0.8559
S 1 1cm	S 6 1cm	0.04159	0.2912	0.14	0.8864
S 1 1cm	S 6 SSS	0.008091	0.2912	0.03	0.9778
S 1 1cm	S 7 1cm	0.08391	0.2912	0.29	0.7732
S 1 1cm	S 7 SSS	0.04137	0.2912	0.14	0.8870
S 1 1cm	S 8 1cm	0.1789	0.2913	0.61	0.5392
S 1 1cm	S 8 SSS	0.1601	0.2913	0.55	0.5827
S 1 1cm	S 9 1cm	0.3333	0.2961	1.13	0.2604
S 1 1cm	S 9 SSS	0.2756	0.2961	0.93	0.3521
S 2 1cm	S 2 SSS	-0.1397	0.05071	-2.75	0.0059
S 2 1cm	S 3 1cm	0.01538	0.04570	0.34	0.7364
S 2 1cm	S 3 SSS	-0.03093	0.04585	-0.67	0.4999
S 2 1cm	S 4 1cm	-0.04010	0.04591	-0.87	0.3825
S 2 1cm	S 4 SSS	-0.04984	0.04584	-1.09	0.2770
S 2 1cm	S 5 1cm	-0.1941	0.04457	-4.35	<.0001
S 2 1cm	S 5 SSS	-0.1817	0.04430	-4.10	<.0001
S 2 1cm	S 6 1cm	-0.1930	0.04461	-4.33	<.0001
S 2 1cm	S 6 SSS	-0.2265	0.04467	-5.07	<.0001
S 2 1cm	S 7 1cm	-0.1507	0.04495	-3.35	0.0008
S 2 1cm	S 7 SSS	-0.1932	0.04481	-4.31	<.0001
S 2 1cm	S 8 1cm	-0.05566	0.04565	-1.22	0.2228
S 2 1cm	S 8 SSS	-0.07450	0.04552	-1.64	0.1018
S 2 1cm	S 9 1cm	0.09875	0.06914	1.43	0.1533
S 2 1cm	S 9 SSS	0.04099	0.06914	0.59	0.5533
S 2 SSS	S 3 1cm	0.1551	0.04561	3.40	0.0007
S 2 SSS	S 3 SSS	0.1088	0.04576	2.38	0.0175
S 2 SSS	S 4 1cm	0.09960	0.04580	2.17	0.0297
S 2 SSS	S 4 SSS	0.08986	0.04575	1.96	0.0496
S 2 SSS	S 5 1cm	-0.05436	0.04445	-1.22	0.2214
S 2 SSS	S 5 SSS	-0.04201	0.04419	-0.95	0.3419
S 2 SSS	S 6 1cm	-0.05329	0.04451	-1.20	0.2313
S 2 SSS	S 6 SSS	-0.08679	0.04457	-1.95	0.0516
S 2 SSS	S 7 1cm	-0.01097	0.04485	-0.24	0.8068
S 2 SSS	S 8 1cm	0.08404	0.04552	1.85	0.0649
S 2 SSS	S 8 SSS	0.06520	0.04540	1.44	0.1510
S 2 SSS	S 9 1cm	0.2384	0.06907	3.45	0.0006
S 2 SSS	S 9 SSS	0.1807	0.06907	2.62	0.0089
S 3 1cm	S 3 SSS	-0.04631	0.03866	-1.20	0.2310
S 3 1cm	S 4 1cm	-0.05548	0.03942	-1.41	0.1594
S 3 1cm	S 4 SSS	-0.06522	0.03933	-1.66	0.0973

S 3 1cm	S 5 1cm	-0.2094	0.03765	-5.56	<.0001
S 3 1cm	S 5 SSS	-0.1971	0.03730	-5.28	<.0001
S 3 1cm	S 6 1cm	-0.2084	0.03752	-5.55	<.0001
S 3 1cm	S 6 SSS	-0.2419	0.03766	-6.42	<.0001
S 3 1cm	S 7 1cm	-0.1661	0.03806	-4.36	<.0001
S 3 1cm	S 7 SSS	-0.2086	0.03790	-5.50	<.0001
S 3 1cm	S 8 1cm	-0.07104	0.03888	-1.83	0.0678
S 3 1cm	S 8 SSS	-0.08988	0.03877	-2.32	0.0205
S 3 1cm	S 9 1cm	0.08336	0.06515	1.28	0.2008
S 3 1cm	S 9 SSS	0.02561	0.06515	0.39	0.6943
S 3 SSS	S 4 1cm	-0.00917	0.03958	-0.23	0.8168
S 3 SSS	S 4 SSS	-0.01891	0.03947	-0.48	0.6319
S 3 SSS	S 5 1cm	-0.1631	0.03781	-4.31	<.0001
S 3 SSS	S 5 SSS	-0.1508	0.03746	-4.02	<.0001
S 3 SSS	S 6 1cm	-0.1621	0.03768	-4.30	<.0001
S 3 SSS	S 6 SSS	-0.1956	0.03781	-5.17	<.0001
S 3 SSS	S 7 1cm	-0.1197	0.03822	-3.13	0.0017
S 3 SSS	S 7 SSS	-0.1623	0.03807	-4.26	<.0001
S 3 SSS	S 8 1cm	-0.02473	0.03903	-0.63	0.5265
S 3 SSS	S 8 SSS	-0.04357	0.03892	-1.12	0.2630
S 3 SSS	S 9 1cm	0.1297	0.06525	1.99	0.0470
S 3 SSS	S 9 SSS	0.07192	0.06525	1.10	0.2704
S 4 1cm	S 4 SSS	-0.00974	0.03931	-0.25	0.8043
S 4 1cm	S 5 1cm	-0.1540	0.03820	-4.03	<.0001
S 4 1cm	S 5 SSS	-0.1416	0.03786	-3.74	0.0002
S 4 1cm	S 6 1cm	-0.1529	0.03800	-4.02	<.0001
S 4 1cm	S 6 SSS	-0.1864	0.03813	-4.89	<.0001
S 4 1cm	S 7 1cm	-0.1106	0.03847	-2.87	0.0041
S 4 1cm	S 7 SSS	-0.1531	0.03830	-4.00	<.0001
S 4 1cm	S 8 1cm	-0.01556	0.03942	-0.39	0.6932
S 4 1cm	S 8 SSS	-0.03440	0.03929	-0.88	0.3814
S 4 1cm	S 9 1cm	0.1388	0.06528	2.13	0.0335
S 4 1cm	S 9 SSS	0.08109	0.06528	1.24	0.2143
S 4 SSS	S 5 1cm	-0.1442	0.03814	-3.78	0.0002
S 4 SSS	S 5 SSS	-0.1319	0.03775	-3.49	0.0005
S 4 SSS	S 6 1cm	-0.1431	0.03791	-3.78	0.0002
S 4 SSS	S 6 SSS	-0.1767	0.03804	-4.64	<.0001
S 4 SSS	S 7 1cm	-0.1008	0.03840	-2.63	0.0087
S 4 SSS	S 7 SSS	-0.1434	0.03822	-3.75	0.0002
S 4 SSS	S 8 1cm	-0.00582	0.03936	-0.15	0.8826
S 4 SSS	S 8 SSS	-0.02466	0.03923	-0.63	0.5297
S 4 SSS	S 9 1cm	0.1486	0.06523	2.28	0.0228
S 4 SSS	S 9 SSS	0.09083	0.06523	1.39	0.1639
S 5 1cm	S 5 SSS	0.01236	0.03588	0.34	0.7306
S 5 1cm	S 6 1cm	0.001074	0.03635	0.03	0.9764
S 5 1cm	S 6 SSS	-0.03243	0.03648	-0.89	0.3742
S 5 1cm	S 7 1cm	0.04339	0.03683	1.18	0.2388
S 5 1cm	S 7 SSS	0.000853	0.03665	0.02	0.9814
S 5 1cm	S 8 1cm	0.1384	0.03771	3.67	0.0002
S 5 1cm	S 8 SSS	0.1196	0.03756	3.18	0.0015
S 5 1cm	S 9 1cm	0.2928	0.06434	4.55	<.0001
S 5 1cm	S 9 SSS	0.2351	0.06434	3.65	0.0003
S 5 SSS	S 6 1cm	-0.01128	0.03598	-0.31	0.7539

S 5 SSS	S 6 SSS	-0.04478	0.03613	-1.24	0.2152
S 5 SSS	S 7 1cm	0.03104	0.03648	0.85	0.3950
S 5 SSS	S 7 SSS	-0.01150	0.03630	-0.32	0.7513
S 5 SSS	S 8 1cm	0.1261	0.03740	3.37	0.0008
S 5 SSS	S 8 SSS	0.1072	0.03725	2.88	0.0040
S 5 SSS	S 9 1cm	0.2805	0.06413	4.37	<.0001
S 5 SSS	S 9 SSS	0.2227	0.06413	3.47	0.0005
S 6 1cm	S 6 SSS	-0.03350	0.03601	-0.93	0.3523
S 6 1cm	S 7 1cm	0.04232	0.03663	1.16	0.2480
S 6 1cm	S 7 SSS	-0.00022	0.03644	-0.01	0.9952
S 6 1cm	S 8 1cm	0.1373	0.03768	& 3.64	0.0003
S 6 1cm	S 8 SSS	0.1185	0.03755	3.16	0.0016
S 6 1cm	S 9 1cm	0.2917	0.06425	4.54	<.0001
S 6 1cm	S 9 SSS	0.2340	0.06425	3.64	0.0003
S 6 SSS	S 7 1cm	0.07582	0.03679	2.06	0.0394
S 6 SSS	S 7 SSS	0.03328	0.03660	0.91	0.3632
S 6 SSS	S 8 1cm	0.1708	0.03782	4.52	<.0001
S 6 SSS	S 8 SSS	0.1520	0.03769	4.03	<.0001
S 6 SSS	S 9 1cm	0.3252	0.06431	5.06	<.0001
S 6 SSS	S 9 SSS	0.2675	0.06431	4.16	<.0001
S 7 1cm	S 7 SSS	-0.04254	0.03670	-1.16	0.2464
S 7 1cm	S 8 1cm	0.09501	0.03805	2.50	0.0126
S 7 1cm	S 8 SSS	0.07617	0.03791	2.01	0.0446
S 7 1cm	S 9 1cm	0.2494	0.06453	3.87	0.0001
S 7 1cm	S 9 SSS	0.1917	0.06453	2.97	0.0030
S 7 SSS	S 8 1cm	0.1376	0.03791	3.63	0.0003
S 7 SSS	S 8 SSS	0.1187	0.03776	3.14	0.0017
S 7 SSS	S 9 1cm	0.2920	0.06443	4.53	<.0001
S 7 SSS	S 9 SSS	0.2342	0.06443	3.63	0.0003
S 8 1cm	S 8 SSS	-0.01884	0.03844	-0.49	0.6241
S 8 1cm	S 9 1cm	0.1544	0.06499	2.38	0.0176
S 8 1cm	S 9 SSS	0.09665	0.06499	1.49	0.1371
S 8 SSS	S 9 1cm	0.1732	0.06487	2.67	0.0076
S 8 SSS	S 9 SSS	0.1155	0.06487	1.78	0.0751
S 9 1cm	S 9 SSS	-0.05776	0.08206	-0.70	0.4816